UDK 622'112:519.876.5
Original scientific article/Izvirni znanstveni članek

ISSN 1580-2949
Mater. Tehnol.

RESEARCH ON THE WATER-HOLDING CAPACITY AND MECHANICAL PROPERTIES OF BACKFILL BASED ON A DAMAGE-SOFTENING CONSTITUTIVE MODEL: EFFECTS OF DIFFERENT PERMEABILITY FORCES

RAZISKAVA SPOSOBNOSTI ZADRŽEVANJA VODE IN MEHANSKE LASTNOSTI MATERIALA ZA ZASIPAVANJE, TEMELJEČA NA KONSTITUTIVNEM MODELU MEHČANJA: VPLIV RAZLIČNIH PERMEABILNOSTNIH SIL

Chaoyi Yang[1,2], Zhenggao Huang[2], Wenzhong Sha[2], Heng Huang[1], Rugao Gao[1,3]*

[1]School of Resources and Safety Engineering, Central South University, Changsha, Hunan 410083, China
[2]Yunnan Diqing Nonferrous Metals Co., Ltd, Yunnan, Shangri-La 674400, China
[3]School of Resource & Environment and Safety Engineering, Hunan University of Science and Technology, Xiangtan 411201, China

Prejem rokopisa – received: 2024-08-26; sprejem za objavo – accepted for publication: 2024-12-02

doi:10.17222/mit.2024.1285

This study investigates the application of tailings backfill through a series of centrifugal and pore characteristic tests. To align with the material's structural properties, a specialized test mold was developed, enabling the preparation of tailings backfill model samples with varying concentrations and proportions. Employing centrifugation and nuclear magnetic resonance (NMR), the study determined the optimal centrifugal force and the T2 critical value for the backfill material. By simulating seepage pressures induced by different centrifugal speeds, uniaxial compression mechanical tests were conducted to analyze the effects of seepage forces on the deformation characteristics and failure modes of the backfill. The results revealed that as seepage force increased, the stress-strain behavior of the samples was altered, with failure modes transitioning from tensile failure to shear failure. This shift was accompanied by an increase in the crack propagation and morphological complexity. Based on these findings, a damage-softening constitutive model incorporating penetration forces was established and validated against experimental data, demonstrating strong agreement. This model provides a robust framework for analyzing uniaxial compression mechanics of backfill materials under varying penetration forces. The outcomes of this research provide valuable insights into high-gravity centrifugal simulations and underground seepage tests, contributing significantly to the design and safety evaluation of tailings backfill systems.

Keywords: backfill, centrifugal simulation, osmotic pressure, mechanical properties

V članku avtorji opisujejo študijo uporabe zasipavanja z jalovino s pomočjo vrste centrifugalnih testov in testov poroznosti. Da bi se avtorji seznanili s strukturnimi lastnostmi materiala so razvili poseben model za preizkušanje, ki je omogočal pripravo vzorcev jalovine za zasipavanje z različnimi koncentracijami in deleži. Z uporabo centrifugiranja in tehnik jedrske magnetne resonance (NMR; angl.: nuclear magnetic resonance) so avtorji določili optimalno centrifugalno silo in kritično vrednost strižne napetosti T2 izbranega materiala za zasipavanje. S simuliranjem induciranega tlaka pronicanja z različnimi centrifugalnimi hitrostmi in enoosnimi mehanskimi preizkusi so avtorji analizirali učinke sil na deformacije in načine porušitve zasipa. Rezultati preizkusov in simulacij so pokazali, da sila pronicanja narašča in napetostno deformacijsko stanje se spremeni s prehodom z nateznega v strižni način porušitve. Ta premik oziroma prehod je povezan s povečanjem hitrosti napredovanja razpok in morfološko kompleksnostjo. Na osnovi teh ugotovitev so avtorji te raziskave zgradili konstitutivni model »poškodba v odvisnosti od mehčanja« (angl.: damage-softening constitutive model) z vključitvijo penetracijskih sil. Nadalje so model ovrednotili v primerjavi z eksperimentalnimi podatki. Ugotovili so dobro ujemanje modela s preizkusi. Ta model je robustno ogrodje za analiziranje enoosne tlačne mehanike materialov za zasipanje v pogojih različnih penetracijskih sil. Ugotovitve te raziskave dajejo pomemben vpogled v centrifugalne simulacije z veliko gravitacijo. Podzemni testi zasipavanja pomembno prispevajo k ocenjevanju dizajna in varnosti sistemov za zasipavanje.

Ključne besede: zasipavanje, centrifugalna simulacija, osmotski tlak, mehanske lastnosti

1 INTRODUCTION

In order to cope with the rapid economic development in recent years, the metal mining industry has been pursuing safe, ecological, and efficient mining methods. In the process of metal mining, it is inevitable to disturb the surrounding rock strata and produce hidden dangerous empty areas. The filling mining method effectively reduces the influence of rock pressure on the stability of the goaf. However, research on filling mining mostly focuses on filling materials, slurry concentration ratio, pipeline transportation, etc., while often ignoring the various effects of the complex underground environment on the backfill, resulting in significant potential safety hazards in underground operations. Groundwater seepage is one of the important factors affecting the damage of the pore structure of backfill. Seepage pressure exerts a

*Corresponding author's e-mail:
gaorgcsu@163.com (Rugao Gao)

long-term wetting effect on the backfill, causing damage and softening to its internal pore structure, which then leads to changes in mechanical properties caused by the deformation of the internal pore skeleton.[1] Most research on damage softening lacks consideration of the influence of the seepage force on porous media backfill. Instead, factors such as concentration ratio and filling materials are often analyzed to study its mechanical behavior, neglecting the influence of the groundwater environment. Therefore, studying the damage softening of the pore structure of the backfill under seepage force is particularly important, providing significant guiding value for engineering practice.

The mechanical properties of backfill have been extensively investigated by scholars both domestically and internationally. M. Z. Emad examined the mechanical properties of cemented backfill under blasting vibration, focusing on filling times, filling interval time, and filling surface.[2] J. Li broadened this research by considering various backfill material types and exploring their mechanical characteristics, providing valuable insights into filling process indices and surface subsidence associated with different materials.[3] Li also conducted numerical simulations based on the long-term mechanical parameters of cement backfill, elucidating paste filling mining patterns beneath highways and slopes.[4] O. Nasir et al. comprehensively assessed the influence of temperature and varying aggregate dosages on the early compressive strength of backfill.[5] A. Ghirian et al. further investigated the fundamental mechanical properties of the backfill within a coupled THMC (thermo-hydro-mechanical-chemical) environment.[6,7] Notably, while prior studies on the uniaxial compressive mechanical properties of backfill have primarily focused on external environmental factors, materials, temperature, and aggregate, the mechanical response of backfill under varying infiltration forces remains underexplored. This aspect warrants further investigation to enhance the current understanding.

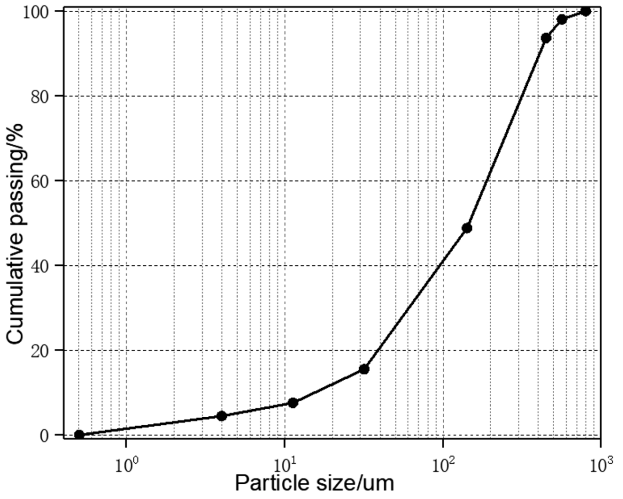

Figure 1: Tail sand particle size distribution curve

Constitutive models of rock and ore bodies affected by water have been analyzed in several recent studies. Most of these investigations are based on the Lemaitre strain equivalence hypothesis.[8,9] W. G. Cao et al. established a statistical constitutive model of rock damage to simulate the entire process of rock strain softening deformation and fracture under varying confining pressures.[10,11] Building on years of research into rock damage softening constitutive models, unified rock damage constitutive models were developed, capable of cosidering the softening and hardening characteristics of rock under different confining pressures.[12,13] Complementing this work, Cao et al. formulated an elastoplastic damage statistical constitutive model rooted in the probability theory and damage mechanics. This model considers the failure, damage, and elastoplastic deformation of rock under load.[14] Meanwhile, J. Zhang et al. introduced a rock strain softening model that incorporates the impact of confining pressure.[15,16] This model uses parameters such as the brittle modulus coefficient, strength degradation index, and dilatancy index. Their study further employed FLAC to simulate the strain softening behavior and permeability evolution of Balikun sandstone under different confining pressures. Lastly, Y. K. Lee et al. proposed a straightforward numerical approach for the elastoplastic analysis of circular tunnels in strain-softening rock masses.[17] Their method assumes that all strength parameters are linear functions of plastic deviatoric strain, providing a concise yet effective framework for tunnel design and analysis in such geological conditions.

Historically, research on the damage constitutive behavior of samples has primarily focused on rock and ore bodies, with limited studies addressing the damage softening constitutive model of backfill under varying permeability.[18] Some studies have not considered the influence of external forces on the backfill itself, and the complexity and unclear determination methods of model parameters hinder engineering applications. Centrifugal simulation experiments are employed in this study to simulate seepage field effects and accelerate the damage and failure of backfill samples under a seepage action. Additionally, based on the Weibull distribution law of rock microelement damage failure, a statistical constitutive model for the damage softening of samples under a seepage force is developed and validated against experimental data. The findings provide valuable references for high-gravity centrifugal simulations and underground seepage tests.

2 MATERIALS AND METHOD

2.1 Testing materials

The raw materials used for the backfill samples consisted of tailings, cement, and water. P.C42.5 Portland cement was utilized to preserve the internal pore structure of the samples during high-speed centrifugation.

The tailings were sourced from a mine in Hunan after undergoing pressure filtration. Their particle size was analyzed using a laser particle size analyzer, with the particle size distribution curve displayed in **Figure 1**. The primary chemical elements of the tailings are listed in **Table 1**.

Table 1: Tailings of the main chemical elements

Ingredient	O	Mg	Al	S	Ca
Content (%)	42.5	5.695	0.781	0.676	33.02
Ingredient	Mn	Fe	Cu	As	Pb
Content (%)	0.468	1.316	0.014	0.13	0.179

According to the test results, the unevenness coefficient of the tailings is 10.3, exceeding 5, while the curvature coefficient is 1.27, falling between 1 and 3. These values indicate that the particle size distribution of the tailings is wide, making them favorable for compaction. Backfill composed of tailings with a wide particle size distribution demonstrates good integrity.[19–21] Consequently, this material is well-suited for the experiment.

2.2 Sample preparation

Experimental samples were fabricated using tailings, water, cement, and other materials sourced from a mining operation. Backfill samples were prepared with cement-to-tailing ratios of 1:4, 1:8, and 1:12, and mass concentrations of (71, 74 and 80) %, respectively. A customized mold with a sample size of $\phi 12 \times 24$ mm was employed. **Figure 2** illustrates geometric specifications and physical appearance of the specimens. In this study, a total of eight test groups, labeled A to H, were conducted, with each group comprising multiple samples. After sample preparation, the specimens were cured for 28 days in a curing box maintained at a temperature of 20 °C and a humidity level exceeding 95 %.

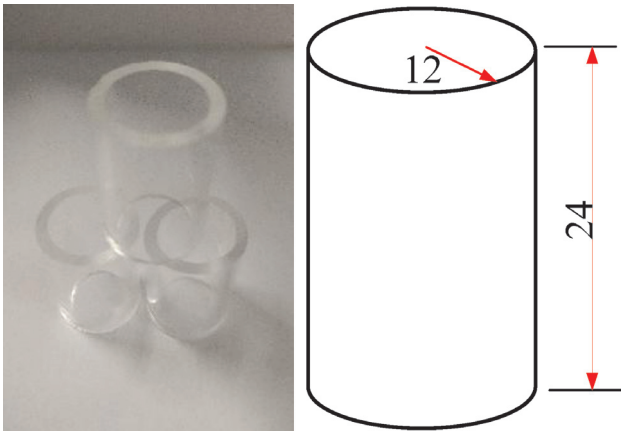

Figure 2: Specimen geometry and physical parameters

2.3 Testing methods

A general flowchart about the experimental process and purpose is presented in **Table 2** to help the readers understand the experiments and centrifugal tests.

NMR test: After placing a backfill sample in the magnetic field, hydrogen ions resonate by emitting an RF pulse at a specific frequency, absorbing its energy. When the RF pulse is stopped, the hydrogen ions release the absorbed energy, a process detectable through the nuclear magnetic resonance signal. The energy release rates of samples with varying properties differ, and these differences in the signals intuitively reflect the variation in pore water retention. The parameters used were a magnetic field strength of 0.3 T, echo time of 0.301 ms, waiting time of 1500 s, sampling frequency of 200 KHz, and magnet control temperature of 25–35 °C.

Centrifugal separation: Drawing on extensive research into overweight centrifugal model testing, this study employs an 80-1 electric centrifuge to simulate underground seepage conditions.[22,23] During the experiments, eight distinct centrifugal speeds (500, 1000, 1500, 2000, 2500, 3000, 3500, and 4000) min^{-1} were applied to

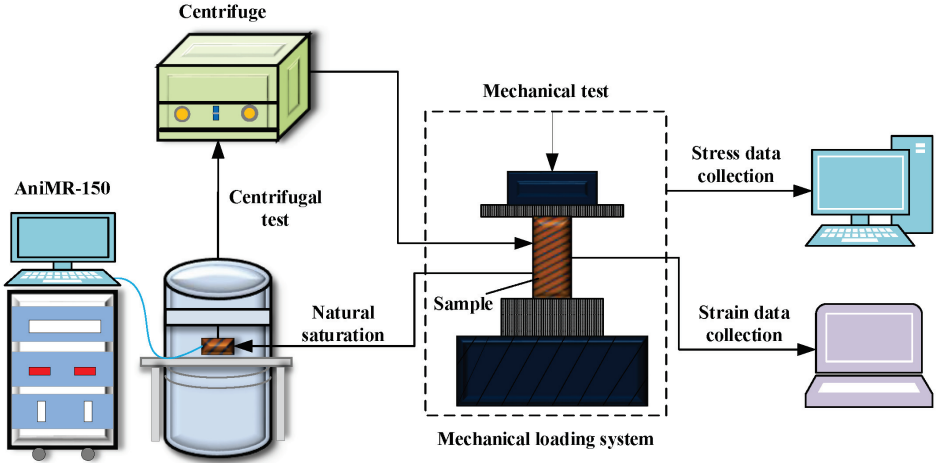

Figure 3: Schematic diagram of the test process

Table 2: Flowchart for experimental set-up and processes

Name	Steps	Set-up	Purpose
Sample preparation	Raw material mixing	Cement-to-tailing ratios of 1:4, 1:8, and 1:12; Mass concentrations of 71, 74, and 80 %	Prepare backfill samples for testing
	Mold formation	Cylindrical mold of f12 × 24 mm	
	Curing	Chamber at 20 °C, 95 % + humidity with 28 d	
Centrifuge simulation	Sample saturation	All samples were completely submerged within water for 6 h	Simulate different seepage forces to assess their effects on backfill
	Centrifugation	Desktop electric centrifuge instrument with speeds of 500–4000 r/min	
NMR	Porosity measurement	NMR measurement for saturated samples	Analyze pore water retention under different seepage conditions
	Pore water retention testing	NMR measurement for samples with different centrifuge speeds; AniMR-150 NMR analysis system	
Uniaxial compression testing	Mechanical performance testing	Instron UTM; displacement control with a speed of 0.5 mm/min	Study mechanical response, including stress-strain characteristics and failure modes
Data analysis	Regression analysis	Regression analysis of mechanical properties	Relationships between parameters studied

the samples to mimic varying penetration forces. Prior to the centrifugal tests, the samples were naturally saturated, and their saturated porosity was measured with precision. The samples were then subjected to different centrifugal speeds during testing. After each centrifugation cycle, a uniaxial compression test was performed to assess the mechanical properties of the samples, facilitating a detailed analysis of pore structure damage in subsequent stages. This experimental process was repeated multiple times, and the specific methodology is depicted in **Figure 3**.

3 RESULTS AND DISCUSSION

To distinguish between free water and bound water in the pores of the samples, determining the T2 cutoff is particularly important. **Figure 4** illustrates the cutoff method (CBVI) for determining the T2 cutoff.[24] This method estimates the BVI (bound volume index) based on the assumption that bound fluid resides in small pores, while movable fluid occupies larger pores. This assumption stems from the relationship between the pore throat size and pore size. Since the T2 value correlates with the pore size, a T2 value can be selected under the assumption that fluids with values smaller than this threshold reside in small pores and are immobile, while those with larger values occupy larger pores and can flow freely. This threshold is referred to as the T2 cutoff. By dividing the T2 distribution, the T2 cutoff applies the MPHI value to represent effective saturation and separates it into two components: the BVI, which represents the saturation of bound fluid, and the FFI (free fluid index), which represents the saturation of movable fluid.

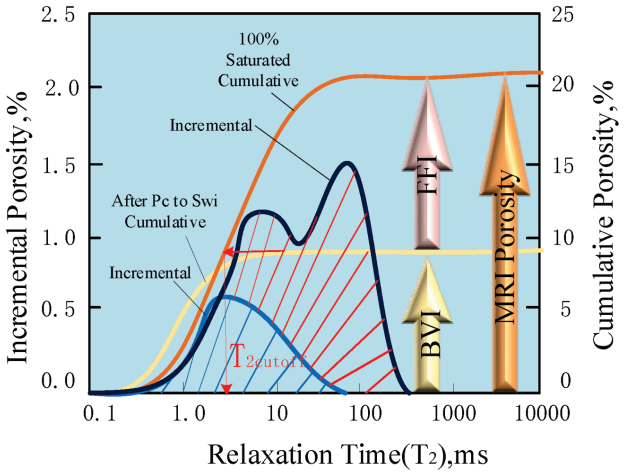

Figure 4: Cutoff method (CBVI) for T2 cutoff

This research investigated the correlation between the pore size distribution and porosity in samples with varying mass concentrations (71, 74, and 80) %. **Figure 5** illustrates the critical values for large and small pores across these concentrations and ratios, revealing a consistent pattern: higher concentrations and smaller critical pore sizes result in a reduced pore volume water retention. The study also identified a positive correlation between a denser distribution of small pores, larger pore sizes, and increased bound water content, which collectively enhance water retention. As the cement-to-tailing ratio increased, the pore size distribution curve shifted towards bimodal characteristics, with distinct spectral peaks representing both large and small pores. Scanning electron microscopy (SEM) was utilized to analyze the microstructure of the backfill, evaluating pore formation and maintenance states. With an increase in the ratio, the T2 spectrum exhibited pronounced bimodal characteristics. The critical pore size decreased, and the pore structure became more diverse. For backfill samples of the same volume, total water retention decreased as the concentration and ratio increased. Furthermore, gelled products formed during hydration progressively filled the in-

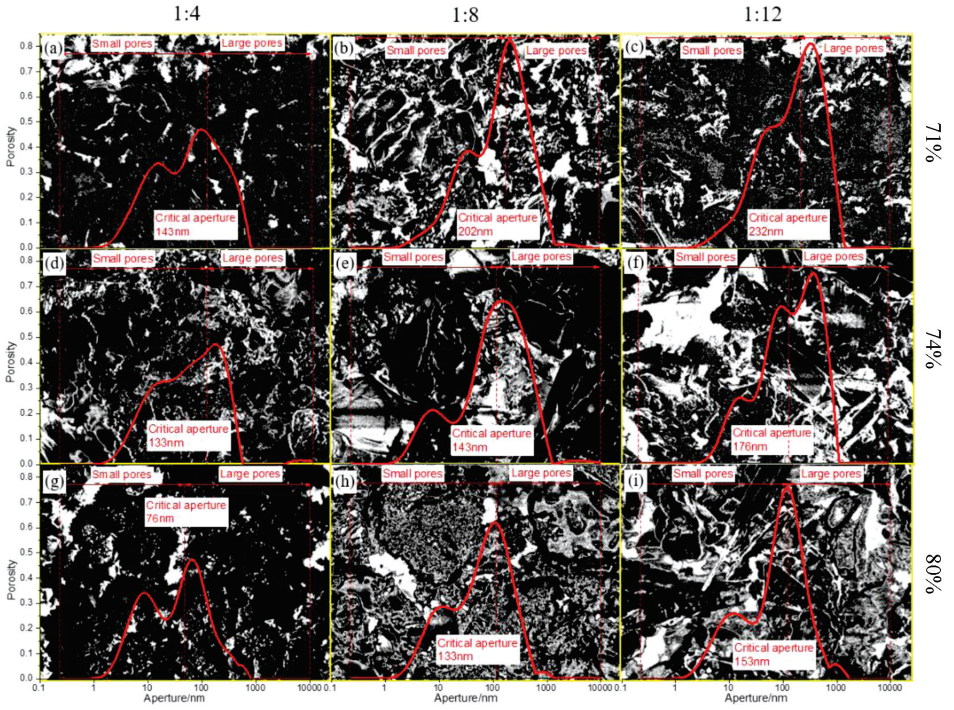

Figure 5: Microscopic pore characteristics of backfill with different concentrations and ratios

ternal pores, with higher cement-to-tailing ratios intensifying the hydration reaction.

3.1 Analysis of stress-strain characteristics under uniaxial compression

As shown in **Figure 6** and **Table 3**, an upward trend in the seepage force correlates with a decrease in the compressive strength of the sample. Simultaneously, the elastic modulus initially increases before decreasing, while the overall range of peak strain diminishes. For example, as the penetration force increased from 0.000445 MPa to 0.028473 MPa, the compressive strength significantly decreased from 1.60 MPa to 0.60 MPa, and the peak strain dropped from 0.0255 to 0.0065. During the loading process, all specimens progressed through four distinct stages: compaction, elasticity, yield, and failure.[25] Before reaching the peak, the stress-strain curve of the specimen exhibited linear behavior. With increasing seepage force, the compaction stage interval in the stress-strain curve first decreased and then increased, while the elastic stage interval shortened. The yield stage became less distinct, and the post-peak stress declined more rapidly, eventually leading to gradual disappearance of the residual strength.

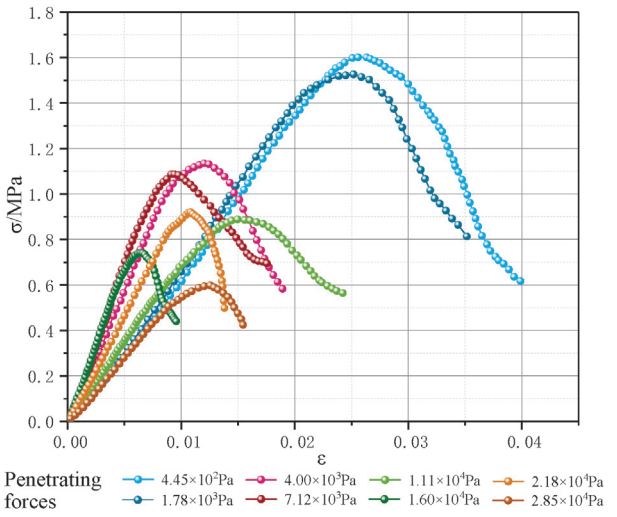

Figure 6: Uniaxial compression stress-strain curve of backfill under different penetrating forces

Table 3: Mechanical parameters of uniaxial compression of backfills with different penetrating forces

No.	Permeability (J)/Pa	Stress (σ)/MPa	Elastic modulus (E)	Strain (ε)
A	J_1	1.60	67.58	0.0255
B	J_2	1.56	74.37	0.0249
C	J_3	1.16	125.42	0.0120
D	J_4	1.09	134.37	0.0093
E	J_5	0.90	72.29	0.0150
F	J_6	0.75	135.97	0.0065
G	J_7	0.93	99.87	0.0100
H	J_8	0.60	62.34	0.0130

3.2 Analysis of the penetration force and mechanical properties of samples

Based on the uniaxial compression test data of backfill samples with varying permeability, three key mechanical characteristic parameters were identified: com-

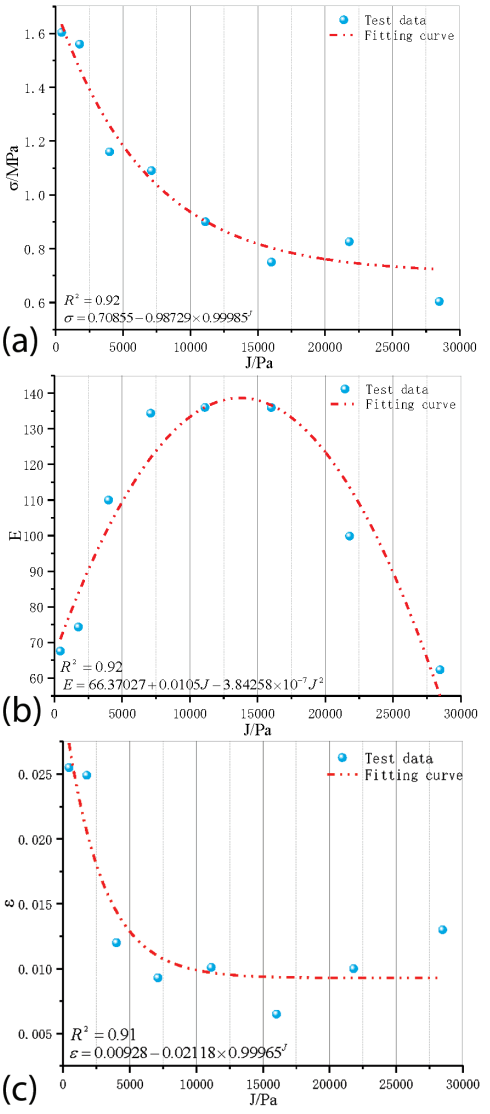

Figure 7: Regression curve of penetration force, compressive strength, elastic modulus and peak strain: a) relationship between compressive strength and permeability, b) relationship between elastic modulus and penetration force, c) relationship between peak strain and seepage force

pressive strength, elastic modulus, and peak strain. The regression analysis diagram depicting the relationships between these three mechanical parameters and penetration force is shown in **Figure 7**. Specifically, the compressive strength and peak strain exhibit a negative exponential function relationship with the penetration force, while the elastic modulus follows a quadratic polynomial relationship. The results of the regression analysis indicate that the measured data of the samples show strong correlation with the regression curve. Functional expressions for the compressive strength, elastic modulus, peak strain, and permeability of backfill samples are as follows, where *a*, *b*, and *c* are fitting parameters:

$$\sigma = a_1 + b_1 \cdot c_1^J \tag{1}$$

$$E = a_2 + b_2 \cdot J + c_2 \cdot J^2 \tag{2}$$

$$\varepsilon = a_3 + b_2 \cdot c_3^J \tag{3}$$

3.3 Failure mode and damage analysis of filling body samples

The mechanical behavior of backfill samples is significantly influenced by varying seepage forces, resulting in diverse failure modes following a load-induced rupture. The failure modes of backfill samples with different permeability values are illustrated in **Figure 8**. Based on experimental observations, samples with permeability values of 0.000445 MPa, 0.00178 MPa, and 0.004004 MPa exhibited tensile failure, characterized by the formation of a solitary tensile crack at the rupture (**Figures 8a** to **8c**). In contrast, samples with permeability values of 0.007118 MPa, 0.011122 MPa, 0.0218 MPa, and 0.028473 MPa exhibited shear failure, manifesting as a conjugate shear fracture pattern. Post-failure, these samples displayed prominent shear cracks (e.g., **Figures 8d**, **8e**, **8g**, and **8h**) accompanied by multiple shear bifurcation cracks.

The results indicate that when the permeability of a backfill sample is below 0.004004 MPa, the failure mode

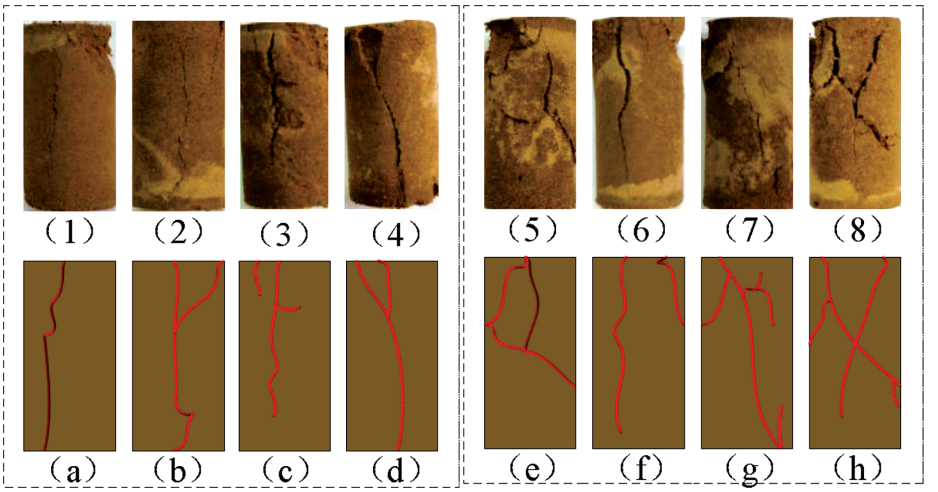

Figure 8: Failure mode and schematic diagram of a filled specimen

is predominantly tensile. However, for permeability values exceeding 0.004004 MPa, the failure mode transitions to shear failure, with the possibility of combined failure. Furthermore, as permeability increases, the number of cracks produced following backfill failure also increases.

It is evident that the compressive strength of a backfill sample decreases under the seepage pressure of water. This decline is accompanied by a reduction in the Poisson's ratio, indicating diminished lateral deformation of the sample. Furthermore, the failure mode transitions from tensile to shear, reflecting a shift in the material's response. Under high permeability conditions, the sample exhibits significant deformation, with a complex stress state characterized by pronounced tensile and shear effects. As a result, the sample sustains severe damage, evidenced by a higher number of post-failure cracks and more intricate crack patterns.

The damage mechanism induced by the water seepage pressure primarily involves two aspects.[26] Firstly, bound water damage arises from water molecules tightly adhered to the mineral surface due to the adsorption force of the mineral exceeding gravity. This adsorption leads to the hydrolysis of soluble salts and colloids, weakening interparticle bonds, reducing friction forces, and ultimately diminishing the overall strength of the sample. Secondly, osmotic damage occurs when the seepage force generated by centrifugation acts on the pores and cracks within the backfill sample. This force subjects microcracks to the hydrostatic pressure, causing them to expand. When combined with the initial water-induced damage, the osmotic pressure exerts superimposed effects during the centrifugal process, exacerbating the damage to the loaded sample.

The phenomenon of the transition of the failure mode of the backfill material from tensile to shear failure has important practical implications for mining safety. Tensile failure generally occurs under low permeability conditions, indicating a higher overall integrity of the backfill. However, when permeability exceeds the critical threshold, shear failure becomes dominant, suggesting a more complex internal stress state, with an increased number of cracks and more intricate crack morphology.

For the design of underground backfill structures, this shift in failure mode highlights the need for a more detailed design and monitoring of the backfill structure in high-permeability environments. An increased occurrence of shear failure could lead to rapid failure of supporting structures, posing potential safety risks. Therefore, in high-permeability conditions, additional reinforcement measures should be considered during the design process, such as increasing the cement content in the backfill material to enhance its shear strength and reduce the likelihood of shear failure.

Furthermore, the findings indicate that the underground seepage pressure significantly contributes to the damage of backfill, especially in mining environments with penetrating water flows. This is crucial for a safety assessment, particularly in mines with complex hydrogeological conditions. Therefore, it is recommend that mine managers increase the monitoring frequency of backfill in areas with a high seepage pressure to prevent collapse risks in mining areas due to shear failure.

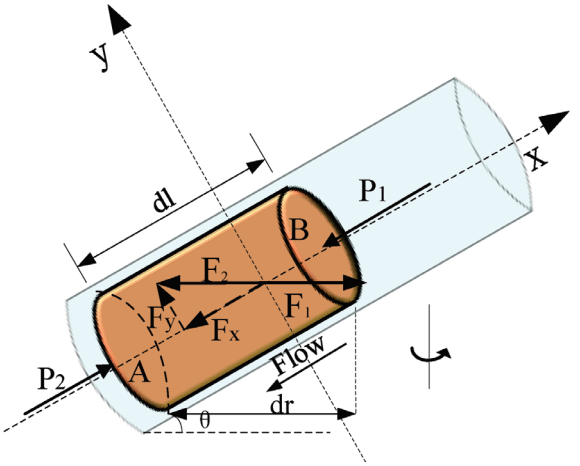

Figure 9: Schematic diagram of a specimen damage unit

4 DAMAGE SOFTENING CONSTITUTIVE MODEL OF A CENTRIFUGAL FIELD

4.1 Centrifugal field mechanics analysis

Based on the calculation model of the seepage force in saturated soil, a damage calculation model for centrifugal interference specimens is established to map the effects of the underground seepage field on backfill.[27] To accurately simulate the mechanical behavior and damage caused by underground seepage on a filling body, the following assumptions are made:

(1) Water molecules during the centrifugal process flow at a uniform speed;

(2) Free water molecules in the pores of the sample flow along the centrifugal force component during the centrifugal process;

(3) The influence of the gravity field is neglected in the analysis of the centrifugal field.

Seepage occurs in a saturated backfill sample when the centrifugal force is sufficient to overcome the resistance of soil particles. As shown in **Figure 9**, in any differential section, the cross-sectional area is *ds*. It is assumed that the pore skeleton and pore water in the sample are separated to isolate the body. The forces acting on the pore water in the sample along the streamline direction include the following components:

(a) the pore pressure difference between A and B sides in the centrifugal field:

$$\Delta p = n\rho r\omega^2 \, \mathrm{d}r\mathrm{d}S \tag{4}$$

In the Equation:

ρ – Water bulk density, Nm^{-3}

n – Sample saturated porosity, %

r – Centrifugal radius, m
ω – Centrifugal angular velocity, rads^{-1}
dS – Sample area microelement

(b) f_x, the component of the centripetal F_1 force in the x direction:

$$f_x = -\rho r\omega^2 \mathrm{d}S \frac{\mathrm{d}r}{\mathrm{d}l} = -\rho r\omega^2 \mathrm{d}r\mathrm{d}S \tag{5}$$

(c) f_1, the total resistance of pore water:

$$f_1 = f_0 \cdot \mathrm{d}S\mathrm{d}l \tag{6}$$

In the Equation, f_0 is the resistance of pore water flow in the unit volume damage sample, which is the reaction force of seepage force.

The pore water pressure on the cross-section of the sample is transmitted uniformly throughout the water body within the sample:

$$-\Delta p(1-n)dS = \rho r\omega^2 (1-n)\mathrm{d}r\mathrm{d}S \tag{7}$$

The buoyancy component, f', on the x-axis produced by the damaged sample particles in the centrifugal field is as follows:

$$f' = -(1-n)\rho r\omega^2 \mathrm{d}l\mathrm{d}S \cdot \frac{\mathrm{d}r}{\mathrm{d}l} = \\ = -(1-n)\rho r\omega^2 \mathrm{d}r\mathrm{d}S \tag{8}$$

The penetration force, J, of the sample in the centrifugal field obtained with the above Equations (4–8) is as follows:

$$J = (1+n)\rho r\omega^2 \cos\theta \tag{9}$$

In the Equation, n is the saturated porosity, obtained with the nuclear magnetic resonance test, the average saturated porosity n = 30.37 %; ρ is the weight of water, ρ = 1 N·m^{-3}; θ is the angle between the sample pipe and the horizontal plane in the centrifuge.

4.2 Damage variable and elastic damage constitutive

When considering the porous medium backfill, which inherently consists of a heterogeneous matrix with randomly distributed microcracks, voids, and other inherent defects, it is essential to acknowledge that the damage inflicted on the microelements of the backfill under seepage force is inherently stochastic. The probability of a microelement within a backfill sample experiencing failure is directly correlated with the magnitude of the seepage force. The proportion of damaged microelements relative to the total microelement population is defined as the damage variable.[28] The criterion for seepage-induced failure of a specimen can be expressed as follows:

$$f(J) = J\varepsilon \tag{10}$$

In the Equation, J is the permeability in the pores of the sample, and ε is the strain. Assuming that the distribution density of the probability of microelement failure with A is B, the damage variable is defined as the failure probability:

$$D = \int_0^J P[f(J)]\mathrm{d}J \tag{11}$$

Microscopic damage usually cannot be observed directly, so it is necessary to establish an expression for conversion. Considering that the stress-strain curve reflects the relationship between stress and strain in a material under external forces or changes, it characterizes the whole process of deformation, from the beginning of deformation, to gradual destruction and the final loss of bearing capacity. During compression, the sample exhibits an elastic deformation stage. Therefore, the elastic damage constitutive model in the seepage field is constructed by combining external factors, internal mechanisms, and the interaction of micro-scale and macro-scale effects. Assuming that the stress-strain relationship of the specimen element follows Hooke's law before failure, the elastic damage constitutive relationship can be formulated as follows:

$$\{\sigma\} = \frac{[c]\{\varepsilon\}}{(1-c_\mathrm{n} D)} \tag{12}$$

In the Equation, $\{\sigma\}$ is the stress vector, $\{\varepsilon\}$ is the strain vector, $[c]$ is the elastic flexibility matrix, and c_n is the variation coefficient, $c_\mathrm{n} \in (0.2)$.

4.3 Construction of damage softening constitutive model

The Weibull probability distribution, widely applicable across various forms, exhibits statistical characteristics similar to those observed in rock compression failure. The characteristic distribution of damage softening in the pore structure of a sample is determined by the interplay of external and internal forces. Consequently, assuming that the failure probability of the sample's microelements conforms with the Weibull function distribution, the microelement damage distribution can be expressed as follows:

$$P[f(J)] = \frac{m}{F_0}\left(\frac{J\varepsilon}{F_0}\right)^{m-1} \exp\left[-\left(\frac{J\varepsilon}{F_0}\right)^m\right] \tag{13}$$

Combining Equations (9), (11) and (13), the damage variable of the sample in the centrifugal field is obtained:

$$D = 1 - e^{-\left(\frac{(1+n)\rho r\varepsilon\omega^2 \cos\theta}{F_0}\right)^m} \tag{14}$$

In the Equation, m and F_0 are randomly distributed variables in the Weibull function.

Combining Equations (12) and (14), the constitutive model expression of the damage stress-strain relationship of a specimen under a compressive load can be obtained:

$$\sigma = E\varepsilon\left[c_\mathrm{n} e^{-\left(\frac{(1+n)\rho r\varepsilon\omega^2 \cos\theta}{F_0}\right)^m} + 1 - c_\mathrm{n}\right] \tag{15}$$

4.4 Determination of damage model parameters

Based on the linear regression, parameters m and F_0 are calculated. A model that is linearly dependent on its unknown parameters is easier to fit compared to a model that is nonlinearly dependent on its unknown parameters, and the resulting estimates exhibit more accurate statistical properties.

Equation (15) is converted as follows:

$$\frac{\sigma}{E\varepsilon}+c_{\mathrm{n}}-1=c_{\mathrm{n}}e^{-\left(\frac{(1+n)\rho r\varepsilon\omega^2\cos\theta}{F_0}\right)^m} \tag{16}$$

By performing a logarithmic transformation on the above Equation, it can be deduced that:

$$\ln c_{\mathrm{n}}-\ln\left(\frac{\sigma}{E\varepsilon}+c_{\mathrm{n}}-1\right)= =\frac{1}{F_0^m}\left((1+n)\rho r\varepsilon\omega^2\cos\theta\right)^m \tag{17}$$

Assuming Equation (17), we derive the following:

$$\frac{1}{F_0^m}=\eta \tag{18}$$

$$\left((1+n)\rho r\varepsilon\omega^2\cos\theta\right)^m=\lambda^m \tag{19}$$

Then the logarithms of (18) and (19) are obtained by taking the logarithms of (17):

$$\ln\left[\ln c_{\mathrm{n}}-\ln\left(\frac{\sigma}{E\varepsilon}+c_{\mathrm{n}}-1\right)\right]=\ln\eta+m\ln\lambda \tag{20}$$

By assuming that:

$$\ln\eta=c \tag{21}$$

$$\ln\lambda=x \tag{22}$$

$$\ln\left[\ln c_{\mathrm{n}}-\ln\left(\frac{\sigma}{E\varepsilon}+c_{\mathrm{n}}-1\right)\right]=y \tag{23}$$

a linear regression equation can be obtained by combining Equations (21), (22) and (23):

$$y=mx+c \tag{24}$$

The linear regression is performed to obtain m, and then F_0 is obtained with $F_0=e^{-c/m}$.

5 MODEL RELIABILITY VERIFICATION

The permeability pressure damage softening constitutive model is verified by uniaxial compression test results. According to the test, permeability J and elastic modulus E are obtained, and parameters m and F_0 are obtained from Equation (24). Specific parameter values are shown in **Table 4**. The coefficient of determination (COD) is defined as follows:

$$COD=R^2=1-\frac{(n-1)\sum_{i=1}^{n}(y_i-y_{iC})^2}{(n-2)\sum_{i=1}^{n}(y_i-y_m)^2} \tag{25}$$

In the Equation, R^2 is the correlation coefficient, n is the number of test data points, $y_i(i=1,2,...,n)$ is the ith data value of y, y_{iC} is the ith calculation model value, and y_{m} is the average value of y_i. Studies have shown that the larger the COD value, the better is the fitting between the model and the experimental data.[29,30]

Table 4: Regression parameter values of backfill specimens with different permeability values

J/Pa	E	c_{n}	F_0	m	R^2
445	67.58	1.2	17	6	0.988
1780	74.37	1.6	73	4	0.989
4004	125.42	0.97	68	4	0.997
7118	134.37	0.75	97	4	0.991
11122	72.29	0.95	240	4	0.991
16016	135.97	0.95	146	5	0.991
21800	99.87	0.98	311	6	0.989
28473	62.34	0.97	451	6	0.995

As depicted in **Figure 10**, the verification results of several backfill samples are presented. The experimental data curve aligns closely with the theoretical model curve, achieving a high coefficient of determination ($R^2 > 0.988$). This strong correlation indicates that the theoretical model effectively captures the damage patterns of the backfill samples under varying seepage forces, as reflected in the stress-strain curve. These findings underscore the validity of the proposed seepage damage softening constitutive model.

A comparative analysis of the theoretical and experimental curves reveals the following advantages of the model:

(1) The model comprehensively encapsulates the damage softening behavior of the backfill sample as a function of the seepage force, providing a detailed representation of its mechanical response under varying conditions;

(2) It accurately reflects the measured stress state of the backfill sample during uniaxial loading, offering a reliable framework for analyzing stress-strain relationship and understanding the material's behavior under load;

(3) The model is characterized by a minimal number of parameters, simplifying its practical application. The elastic modulus (E) and the seepage force (J) can be directly determined through experimentation, while the Weibull distribution parameters (m and F_0) are obtained via linear regression of experimental data. This simplicity facilitates the practical implementation and widespread utilization of the model.

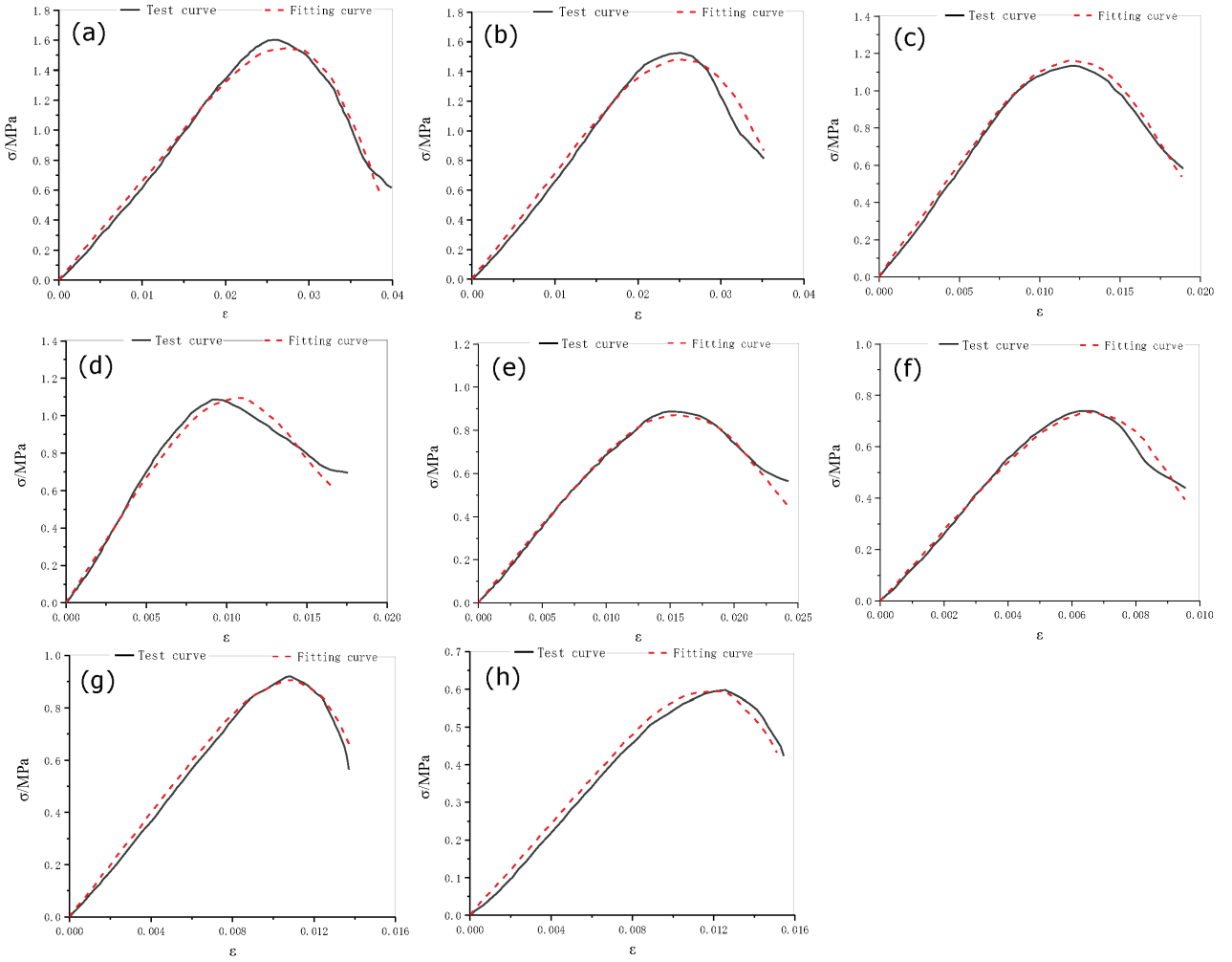

Figure 10: Test curve and theoretical model of different permeability seepage specimens: a) $J_1 = 4.45\times10^2$ Pa, b) $J_2 = 1.78\times10^3$ Pa, c) $J_3 = 4.00\times10^3$ Pa, d) $J_4 = 7.12\times10^3$ Pa, e) $J_5 = 1.11\times10^4$ Pa, f) $J_6 = 1.60\times10^4$ Pa, g) $J_7 = 2.18\times10^4$ Pa, h) $J_8 = 2.85\times10^4$ Pa

6 CONCLUSIONS

This research investigates the influence of an underground seepage field on the pore structure of backfill, which subsequently impacts the strength of the backfill and poses potential engineering safety hazards. To address this, centrifugal response technology is proposed as a method to simulate the seepage effect and accelerate the seepage damage process in backfill samples. Based on the mechanical response analysis, a damage softening constitutive model under centrifugal field conditions is developed. The primary research findings and conclusions are summarized as follows:

(1) With increasing seepage force, the stress-strain curve of a backfill specimen demonstrates the following trends: the compaction stage interval decreases initially and then increases, the elastic stage interval shortens, the yield stage becomes indistinct, the post-peak stress drop rate accelerates, and the residual strength gradually diminishes. The relationships between the compressive strength, peak strain, and penetration force follow a negative exponential function, while the elastic modulus and penetration force exhibit a quadratic polynomial relationship.

(2) The results indicate that when the penetration force of the backfill sample is below 0.004 MPa, the failure mode is tensile. When the penetration force exceeds 0.004 MPa, the failure mode transitions to shear, with the possibility of combined failure. As the penetration force increases, the number of cracks generated after failure rises, and their morphology becomes increasingly complex. The combined effects of initial water-induced damage and superimposed damage caused by seepage pressure exacerbate the overall damage to the loaded specimen. Therefore, the material composition and monitoring in high-permeability environments should be developed to effectively improve the stability of backfill and reduce safety risks during mining operations.

(3) This study derives a damage softening statistical constitutive model for backfill samples with varying permeability. The model is characterized by a minimal number of parameters, which are easy to obtain and exhibit a high degree of fit with experimental data. It is highly ef-

fective for analyzing the uniaxial compressive stress-strain behavior of backfill under different seepage pressure conditions. The relevant model parameters provided in this study facilitate further experimental research and practical applications.

Acknowledgments

This work was financially supported by the National Natural Science Foundation of China (grant no. 52404120).

7 REFERENCES

[1] J. Liu, W. Sui, D. Zhang, Q. Zhao, Durability of water-affected paste backfill material and its clean use in coal mining, J. Clean. Prod., 250 (**2020**), 119576, doi:10.1016/j.jclepro.2019.119576

[2] M. Z. Emad, H. Mitri, C. Kelly, Dynamic model validation using blast vibration monitoring in mine backfill, Int. J. Rock Mech. Min. Sci., 107 (**2018**), 48–54, doi:10.1016/j.ijrmms.2018.04.047

[3] J. Li, E. Yilmaz, S. Cao, Influence of industrial solid waste as filling material on mechanical and microstructural characteristics of cementitious backfills, Constr. Build. Mater., 299 (**2021**), 124288, doi:10.1016/j.conbuildmat.2021.124288

[4] G. Li, G. Z. Deng, J. Ma, Numerical modelling of the response of cemented paste backfill under the blasting of an adjacent ore stope, Constr. Build. Mater., 343 (**2022**), 128051, doi:10.1016/j.conbuildmat.2022.128051

[5] O. Nasir, M. Fall, Coupling binder hydration, temperature and compressive strength development of underground cemented paste backfill at early ages, Tunn. Undergr. Space Technol., 25 (**2010**), 9–20, doi:10.1016/j.tust.2009.09.002

[6] A. Ghirian, M. Fall, Coupled thermo-hydro-mechanical–chemical behaviour of cemented paste backfill in column experiments. Part I: physical, hydraulic and thermal processes and characteristics, Eng. Geol., 164 (**2013**), 195–207, doi:10.1016/j.enggeo.2013.07.011

[7] A. Ghirian, M. Fall, Coupled thermo-hydro-mechanical–chemical behaviour of cemented paste backfill in column experiments. Part II: Mechanical, chemical and microstructural processes and characteristics, Eng. Geol., 170 (**2014**), 11–23, doi:10.1016/j.enggeo.2013.12.006

[8] J. Lemaitre, How to use damage mechanics, Nucl. Eng. Des., 80 (**1984**), 233–245, doi:10.1016/0029-5493(84)90169-9

[9] P. Kittl, G. Diaz, Weibull's fracture statistics, or probabilistic strength of materials: state of the art, Res. Mech., 24 (**1988**), 99–207, doi:10.1016/0921-8181(88)90001-0

[10] W. G. Cao, X. Li, H. Zhao, Damage constitutive model for strain-softening rock based on normal distribution and its parameter determination, J. Cent. South Univ. Technol., 14 (**2007**), 719–724, doi:10.1007/s11771-007-0134-0

[11] Z. L. Wang, Y. C. Li, J. G. Wang, A damage-softening statistical constitutive model considering rock residual strength, Comput. Geosci., 33 (**2007**), 1–9, doi:10.1016/j.cageo.2006.02.011

[12] S. Q. Yang, B. Hu, P. Xu, Study on the damage-softening constitutive model of rock and experimental verification, Acta Mech. Sin., 35 (**2019**), 786–798, doi:10.1007/s10409-018-00833-y

[13] J. Chen, W. Wang, L. Chen, A strain hardening and softening constitutive model for hard brittle rocks, Appl. Sci., 13 (**2023**), 2764, doi:10.3390/app13052764

[14] K. Cao, Y. Li, X. Li, Y. Zhang, Statistical damage model for dry and saturated rock under uniaxial loading based on infrared radiation for possible stress prediction, Eng. Fract. Mech., 260 (**2022**), 108134, doi:10.1016/j.engfracmech.2021.108134

[15] Z. Song, J. Zhang, The effect of confining pressure on mechanical properties in coal and rock: review and new insights, Arab. J. Geosci., 14 (**2021**), 2564, doi:10.1007/s12517-021-08553-7

[16] Y. Xiao, Y. Qiao, M. He, H. Li, T. Cheng, J. Tang, A unified strain-hardening and strain-softening elastoplastic constitutive model for intact rocks, Comput. Geotech., 148 (**2022**), 104772, doi:10.1016/j.compgeo.2022.104772

[17] Y. K. Lee, S. Pietruszczak, A new numerical procedure for elasto-plastic analysis of a circular opening excavated in a strain-softening rock mass, Tunn. Undergr. Space Technol., 23 (**2008**), 588–599, doi:10.1016/j.tust.2007.11.002

[18] Y. Hu, X. Zhang, J. Li, Y. Wang, Experimental study on the influence of hypergravity on the nonlinear flow behaviour in rock fracture, Rock Mech. Rock Eng., 57 (**2024**), 961–978, doi:10.1007/s00603-023-03195-4

[19] T. Belem, M. Benzaazoua, Predictive models for prefeasibility cemented paste backfill mix design, Proc. 3rd Inter. Conf. on Post-Mining, Nancy, France, 2008, 1–12

[20] R. Gao, K. Zhou, J. Zhang, H. Guo, Q. Ren, Research on the dynamic characteristics in the flocculation process of mineral processing tailings, IEEE Access, 7 (**2019**), 129244–129259, doi:10.1109/ACCESS.2019.2939780

[21] E. Sadrossadat, H. Basarir, G. Luo, A. Karrech, R. Durham, A. Fourie, M. Elchalakani, Multi-objective mixture design of cemented paste backfill using particle swarm optimisation algorithm, Miner. Eng., 153 (**2020**), 106385, doi:10.1016/j.mineng.2020.106385

[22] R. Chen, X. Yin, L. Tang, Y. Chen, Centrifugal model tests on face failure of earth pressure balance shield induced by steady state seepage in saturated sandy silt ground, Tunn. Undergr. Space Technol., 81 (**2018**), 315–325, doi:10.1016/j.tust.2018.06.031

[23] T. Wang, Z. Hu, Y. Ji, J. Ma, W. Chen, Centrifugal model test based bearing characteristics and analytical model of uplift pile in combined composite ground, Rock Mech. Rock Eng., 55 (**2022**), 3525–3543, doi:10.1007/s00603-021-02658-0

[24] Y. Zhao, B. Lin, T. Liu, Y. Zheng, Y. Sun, G. Zhang, Q. Li, Multifractal analysis of coal pore structure based on NMR experiment: A new method for predicting T2 cutoff value, Fuel, 283 (**2021**), 119338, doi:10.1016/j.fuel.2020.119338

[25] C. Sun, B. Zhu, T. Luo, K. Liu, T. Wei, S. Yang, Uniaxial compressive mechanical properties and stress–strain model for roller-compacted concrete with initial damage subjected to freeze–thaw cycles, Constr. Build. Mater., 411 (**2024**), 134256, doi:10.1016/j.conbuildmat.2023.134256

[26] X. Liu, J. Chen, B. Liu, S. Wang, Q. Liu, J. Luo, Effects of seepage pressure on the mechanical behaviors and microstructure of sandstone, J. Rock Mech. Geotech. Eng., 16 (**2024**), 2033–2051, doi:10.1016/j.jrmge.2023.08.012

[27] C. Hou, Z. Zhang, X. Yang, Three-dimensional tunnel face stability considering the steady-state seepage in saturated and unsaturated regions with changing water levels, Comput. Geotech., 146 (**2022**), 104741, doi:10.1016/j.compgeo.2022.104741

[28] S. Liu, S. Lu, Z. Wan, J. Cheng, Investigation of the influence mechanism of rock damage on rock fragmentation and cutting performance by the discrete element method, R. Soc. Open Sci., 6 (**2019**), 190116, doi:10.1098/rsos.190116

[29] S. Chen, C. Qiao, Q. Ye, M. U. Khan, Comparative study on three-dimensional statistical damage constitutive modified model of rock based on power function and Weibull distribution, Environ. Earth Sci., 77 (**2018**), 1–8, doi:10.1007/s12665-018-7226-9

[30] H. Lin, J. Feng, R. Cao, S. Xie, Comparative analysis of rock damage models based on different distribution functions, Geotech. Geol. Eng., 40 (**2022**), 301–310, doi:10.1007/s10706-021-01930-3